SOME RECENT APPLICATIONS OF THE SUCTION ANALOGY TO ASYMMETRIC FLOW SITUATIONS

James M. Luckring
NASA Langley Research Center

13

SUMMARY

This paper reviews a recent extension of the suction analogy for estimation of vortex loads on asymmetric configurations. This extension includes asymmetric augmented vortex lift and the forward sweep effect on side edge suction. Application of this extension to a series of skewed wings has resulted in an improved estimating capability for a wide range of asymmetric flow situations. Hence, the suction analogy concept now has more general applicability for subsonic lifting surface analysis.

INTRODUCTION

For lifting surfaces having relatively sharp leading and side edges, the commensurate separation associated with the vortex-lift phenomena can have considerable impact on the performance of high-speed maneuvering aircraft. A detailed knowledge of these flow phenomena, which are referred to as vortex flows, is necessary for proper design and analysis of such aircraft.

For estimating the lift associated with these vortex flows, Polhamus introduced the concept of the leading-edge suction analogy (ref. 1). The suction analogy states that for the separated flows situation, the potential-flow leading-edge suction force becomes reoriented from acting in the chord plane to acting normal to the chord plane (a rotation of 90°) by the local vortex action resulting in an additional normal force. (See insert on fig. 1.) The reasoning is that the force required to maintain the reattached flow is the same as that which had been required to maintain the potential flow around the leading edge.

An application of the suction analogy is shown in figure 1 for a 75° swept sharp-edge delta wing at a low subsonic Mach number taken from reference 2. Both lift as a function of angle of attack and drag due to lift are seen to be well estimated by the analogy. Since the original application, the suction analogy concept has been applied to more general planforms. (See refs. 3 and 4.)

In reference 5, Lamar demonstrated that the suction analogy was not limited to analysis of leading-edge vortex flows, but could be applied wherever singularities in the potential-flow induced velocities produce an edge force. Figure 2, taken from reference 5, illustrates that vortex lift may be expected along streamwise side edges due to the singularities in the sidewash.

Whereas the theories of references 1 to 5 have dealt with estimating the effects of separation-induced vortex flows on longitudinal aerodynamic characteristics for symmetrical configurations having symmetrical loads, it is desirable to have a method which allows for asymmetric configurations such as oblique

or skewed wings, for example, and asymmetric flight conditions such as those associated with sideslip or lateral control.

Accordingly, the present investigation deals with a recent extension of the suction analogy concept to include asymmetric flow situations. To accomplish this analysis, the computer program of references 6 and 7 has been generalized to account for asymmetry resulting in the asymmetric vortex-lattice (AVL) program. Although analysis with this program may be performed on many different types of asymmetric flow situations, as shown in figure 3, this paper will focus on the analysis of wings with geometric asymmetries and, in particular, on untapered skewed wings having separated vortex flows along leading and side edges. The effects of forward sweep on side-edge suction are introduced and the concept of augmented vortex lift as developed in reference 8 is applied to skewed wings.

Subsonic solutions can be obtained with the AVL program for configurations having matrix sizes up to 400 × 400. Operating in FORTRAN extended (FTN) version 4.4, the program requires 74000_8 storage and can solve a 200 singularity configuration in less than 2 minutes on the Control Data Corporation (CDC) 6600 system running under NOS 1.0. Compared with its symmetric progenitor, the program requires 13000_8 more storage, but executes roughly 20 percent faster for the same configuration.

SYMBOLS

A aspect ratio

b wing span

C_D drag coefficient, $\frac{\text{Drag}}{q_\infty S_{ref}}$

$C_{D,o}$ experimental value of drag coefficient at $C_L = 0$

C_L lift coefficient, $\frac{\text{Lift}}{q_\infty S_{ref}}$

$\Delta C_{L,v}$ C_L increment associated with augmented vortex lift

C_l rolling-moment coefficient about reference point, $\frac{\text{Rolling moment}}{q_\infty S_{ref} b}$

$C_{l_\beta} = \frac{\partial C_l}{\partial \beta}$

$C_{l_p} = \frac{\partial C_l}{\partial \left(\frac{pb}{2U}\right)}$

C_{l_r} $= \dfrac{\partial C_l}{\partial\left(\dfrac{rb}{2U}\right)}$

C_m pitching-moment coefficient about reference point which is located at $\dfrac{c_{ref}}{4}$ unless otherwise stated, $\dfrac{\text{Pitching moment}}{q_\infty S_{ref} c_{ref}}$

C_N normal-force coefficient, $\dfrac{\text{Normal force}}{q_\infty S_{ref}}$

C_n yawing-moment coefficient about reference point, $\dfrac{\text{Yawing moment}}{q_\infty S_{ref} b}$

C_{n_β} $= \dfrac{\partial C_n}{\partial \beta}$

C_{n_p} $= \dfrac{\partial C_n}{\partial\left(\dfrac{pb}{2U}\right)}$

C_{n_r} $= \dfrac{\partial C_n}{\partial\left(\dfrac{rb}{2U}\right)}$

C_S leading-edge suction-force coefficient, $K_{v,le}|\sin\alpha|\sin\alpha$

C_T leading-edge thrust-force coefficient, $C_S \cos\Lambda$

C_Y leading-edge side-force coefficient, $C_S \sin\Lambda$

$C_{Y,se}$ side-edge side-force coefficient

c streamwise chord

$\tilde{c}$ characteristic length used in determination of $\bar{K}_{v,se}$

c_s section suction-force coefficient, $\dfrac{\text{Section suction force}}{q_\infty c}$

c_t section thrust-force coefficient, $\dfrac{\text{Section thrust force}}{q_\infty c}$

c_y section side-force coefficient, $\frac{\text{Section side force}}{q_\infty c}$

$f_{y,i}$ elemental side force

K_p potential-lift factor, $\frac{\partial\left(C_{N,p}\right)}{\partial(\sin\alpha\cos\alpha)}$

$K_{v,le}$ leading-edge-vortex lift factor,

$$\partial\left(\frac{\frac{\text{Leading-edge suction force from one edge}}{q_\infty S_{ref}}}{\partial \sin^2\alpha}\right)$$

$K_{v,se}$ side-edge-vortex lift factor,

$$\partial\left(\frac{\frac{\text{Side-edge suction force from one edge}}{q_\infty S_{ref}}}{\partial \sin^2\alpha}\right)$$

$\bar{K}_{v,se}$ augmented-vortex lift factor, $\frac{K_{v,le}}{(b)\sec\Lambda}\tilde{c}$

M free-stream Mach number

p roll rate, rad/sec

q_∞ free-stream dynamic pressure

r yaw rate, rad/sec

S surface area

U free-stream velocity

u induced velocity in x-direction at point (x,y)

v induced velocity in y-direction at point (x,y)

$\bar{x}$ centroid

α angle of attack

β angle of sideslip

γ distributed bound vorticity at point (x,y)

δ distributed trailing vorticity at point (x,y)

η spanwise location in percent semispan

Λ leading-edge sweep angle, positive for sweepback

Subscripts:

av average

c centroid

i particular item of location

le leading edge

p potential or attached flow

r root

ref reference; for S, true wing area; for c, mean geometric chord

se side edge

tot total

vle vortex effect at leading edge

vse vortex effect at side edge

RESULTS AND DISCUSSION

Modified Vortex-Lattice Method

In the analysis of separation-induced vortex flow effects for symmetric configurations by the method of references 6 and 7, the following equations are used to compute C_L, C_D, C_m, and C_l:

$$C_{L,tot} = \overbrace{K_p \sin\alpha \cos^2\alpha}^{C_{L,p}} + \overbrace{K_{v,le}|\sin\alpha| \sin\alpha \cos\alpha}^{C_{L,vle}} + \overbrace{K_{v,se}|\sin\alpha| \sin\alpha \cos\alpha}^{C_{L,vse}} \quad (1)$$

or

$$C_{L,tot} = K_p \sin\alpha \cos^2\alpha + K_{v,tot}|\sin\alpha| \sin\alpha \cos\alpha \quad (2)$$

$$C_D = C_{D,o} + C_L \tan \alpha = C_{D,o} + K_p \sin^2 \alpha \cos \alpha + K_{v,tot} \sin^3 \alpha \tag{3}$$

$$C_{m,tot} = \overbrace{K_p \sin \alpha \cos \alpha \frac{\bar{x}_{c,p}}{c_{ref}}}^{C_{m,p}} + \overbrace{K_{v,le} |\sin \alpha| \sin \alpha \frac{\bar{x}_{c,le}}{c_{ref}}}^{C_{m,vle}}$$

$$+ \overbrace{K_{v,se} |\sin \alpha| \sin \alpha \frac{\bar{x}_{c,se}}{c_{ref}}}^{C_{m,vse}} \tag{4}$$

$$C_{l,tot} = \overbrace{K_p \sin \alpha \cos \alpha \frac{\bar{y}_{c,p}}{b}}^{C_{l,p}} + \overbrace{K_{v,le} |\sin \alpha| \sin \alpha \frac{\bar{y}_{c,le}}{b}}^{C_{l,vle}}$$

$$+ \overbrace{K_{v,se} |\sin \alpha| \sin \alpha \frac{\bar{y}_{c,se}}{b}}^{C_{l,vse}} \tag{5}$$

where the particular $\bar{x}$ terms represent the distance between the appropriate centroid and the reference point X_{ref} taken to be the quarter chord of the mean geometric chord. The potential flow lift term K_p is computed from the symmetric vortex lattice and the vortex lift terms, $K_{v,le}$ and $K_{v,se}$, are computed from the symmetric potential flow solution by using the suction analogy. The application of this technique is not limited, however, to symmetric conditions and should be applicable to asymmetric conditions providing the appropriate values of K_p and K_v can be obtained.

The asymmetric vortex-lattice computer program was developed from its symmetric progenitors (refs. 6 and 7) to compute potential flow solutions about arbitrary thin asymmetric configurations. Once the asymmetric potential-flow solution (and, hence, K_p) is known, the suction analogy may be invoked to compute corresponding asymmetric vortex lift terms, $K_{v,le}$ and $K_{v,se}$. The analysis technique of equations (1) to (5) may now be employed by using the K_p and K_v quantities as computed from the asymmetric potential flow.

In applying this analysis to a series of sharp-edged skewed wings, some additional aerodynamic effects associated with these wings had to be considered. The following sections describe these effects and present the analysis.

Effects of Forward Sweep on Side-Edge Suction

In the computation of side-edge vortex lift by the method of reference 7, the portion of the wing inboard of the side edge is assumed to contribute to the side force acting on the side edge. For sweptback wings, this technique does not lead to complications with the leading-edge forces in that the leading-edge side force and the side-edge side force do not interact with one another. However, in the instance of forward sweep such as for a skewed wing as illustrated in the upper left part of figure 4, the leading-edge side force and the side-edge side force act in opposition to one another across an elemental spanwise strip. A more detailed illustration of the forward-swept semispan is presented in the upper right portion of figure 4. Here the leading-edge and side-edge section side forces are seen to oppose one another along a representative elemental spanwise strip; as a result, there is a region of positive elemental side force and a region of negative elemental side force. The distribution of elemental side force along the representative spanwise strip is shown in the lower right part of figure 4.

The change of sign of the elemental side force would tend to imply that the positive elemental side forces act on the side edge while the negative elemental side forces act on the leading edge. A comparison of the leading-edge side-force distribution computed by integrating the negative elemental side forces on the sweptforward semispan with the side-force component of the leading-edge thrust force on the sweptforward semispan is presented in the lower left part of figure 4. The agreement tends to substantiate the implication that the negative elemental side forces are in actuality the side-force component of the leading-edge thrust. This force has already been accounted for in the present method by computing the leading-edge thrust and using the secant relationship of the leading-edge sweep to compute the resultant leading-edge suction. Accordingly, to compute the side-edge force on the sweptforward semispan properly, only the positive elemental side forces inboard of the side edge are integrated.

Augmented Vortex Lift

In reference 8, Lamar introduced the concept of augmented vortex lift for estimation of loads rising from a vortex persisting downstream and passing over lifting surfaces such as the aft part of a wing or a tail. This persistence results in an additional vortex lift term $\Delta C_{L,v}$ unaccounted for by the suction analogy which deals only with the forces generated along a particular edge.

Figure 5 illustrates the concept of augmented vortex lift applied to a skewed wing. In applying the method of reference 8, the leading-edge vortex lift factor $K_{v,le}$ developed along the leading-edge length $b \sec \Lambda$ persists over a portion of the wing aft of the leading edge $\tilde{c}$ taken to be the tip chord. This condition results in the additional vortex lift factor

$$\bar{K}_{v,se} = \left(\frac{K_{v,le}}{b \sec \Lambda}\right)\tilde{c} \qquad (6)$$

which has the same angle-of-attack dependence as the other vortex terms. Since the chordwise centroid of side-edge vortex lift distributions is generally near the midpoint of the tip chord, the chordwise centroid of the augmented vortex lift factor is taken to be the midpoint of the tip chord. It should be noted that the augmented vortex lift occurs only on the downwind side edge.

As long as the leading-edge vortex remains in the vicinity of the leading edge, it will pass over a region of the wing aft of the leading edge that has a length roughly equal to the tip chord. The choice of the tip chord for $\tilde{c}$ is consistent with the assumption employed in this analysis that the vortex loads act along the edge from which they originate. This assumption is valid as long as a substantial amount of vortex growth and subsequent inboard movement of the vortex core is not encountered.

Skewed Wing Analysis

Figure 6 presents a comparison between a swept and a skewed wing of the span load and section suction distributions. Although in each case the total loads remain essentially the same for both wings, the distribution of the load is seen to shift for the skewed wing to the sweptback semispan. A comparison between the separated flow theory and experiment for these two wings is shown in figure 7. Data for the swept wing was obtained from reference 9. Although the lift is well predicted in both cases, the augmented pitching moment for the skewed wing is seen to predict the data well up to an angle of attack of approximately 6°; above this angle it overpredicts the data. The discrepancy between theory and data for the skewed wing pitching moment may partly be attributed to excessive vortex growth and subsequent movement of the vortex core inboard as the angle of attack is increased. This behavior is illustrated in figure 8. In the application of the suction analogy, the vortex loads are assumed to be edge forces and no angle-of-attack dependence of the centroids is computed. Moreover, as the vortex moves inboard, the amount of the wing over which the vortex passes giving rise to the augmented term decreases and may even become negative. Hence, the present application of augmentation for moment calculation may only be applicable for low to moderate angles of attack depending on how much variance $\tilde{c}$ will experience as a function of α.

Figures 9 to 11 present lift, pitching-moment, and rolling-moment characteristics of several skewed wings having an aspect ratio of one and varying leading-edge sweep. A configuration having a cylindrical fuselage 0.24b in diameter and $1.85c_r$ in length with a midwing is also presented.

In all cases, the lift was well estimated by including the edge-vortex and augmented-vortex contributions. Similarly, the nonlinear pitching-moment trends were well predicted by the edge-vortex contribution, the augmentation enhancing the prediction at low to moderate angles of attack. The potential-flow pitching-moment curve is seen to have a sign opposite from that of the data. Rolling moments were well predicted by the edge-vortex terms up to approximately 8° where the inboard vortex movement became significant; this condition caused a

sign reversal in the data except for the wing-fuselage configuration. The primary effect of the fuselage is to break the leading-edge vortex into two pieces, one emanating from the wing apex and bending downstream at the right-wing fuselage juncture and the other emanating from the left leading-edge fuselage juncture and bending downstream at the left wing tip. Regenerating the leading-edge vortex with the fuselage substantially decreases the extent of inboard movement of the vortex as exhibited by the agreement between theory and experiment for the pitching- and rolling-moment coefficients of figures 10 and 11.

Figures 12 to 14 present the lift, pitching-moment, and rolling-moment characteristics of several skewed wings of varying aspect ratio. As in the previous case, the lift was well predicted for the three wings. The experimental pitching moments are well predicted by including the augmented term but the experimental rolling moments still depart from the theory at approximately 6°. Hence, for these wings the chordwise distribution of the load is being well estimated whereas the spanwise distribution of the load can be estimated only as long as a substantial inboard movement of the vortex is not encountered.

CONCLUDING REMARKS

This paper has presented a recent extension of the suction analogy for the estimation of potential and vortex loads on asymmetric configurations. The analysis has been accomplished by the development and application of an asymmetric vortex-lattice computer program which may be used to compute the potential and vortex loads on asymmetric configurations. In applying this analysis to a series of sharp-edge skewed wings, the effects of forward sweep on side-edge suction and of a skewed geometry on augmented vortex lift have been accounted for. Total loads have been well predicted whereas pitching and rolling moments have been well predicted only as long as the assumption that the vortex loads act along the edge from which the vortex has originated is not violated. Hence, the suction analogy concept may now be applied to a wider range of isolated planforms resulting in an improved estimating capability of separation-induced vortex flow.

REFERENCES

1. Polhamus, Edward C.: A Concept of the Vortex Lift of Sharp-Edge Delta Wings Based on a Leading-Edge-Suction Analogy. NASA TN D-3767, 1966.

2. Wentz, William H., Jr.; and Kohlman, David L.: Wind Tunnel Investigations of Vortex Breakdown on Slender Sharp-Edged Wings. Rep. FRL 68-013 (Grant NGR-17-002-043), Univ. of Kansas Center for Research, Inc., Nov. 27, 1969. (Available as NASA CR-98737.)

3. Polhamus, Edward C.: Charts for Predicting the Subsonic Vortex-Lift Characteristics of Arrow, Delta, and Diamond Wings. NASA TN D-6243, 1971.

4. Polhamus, Edward C.: Predictions of Vortex-Lift Characteristics by a Leading-Edge Suction Analogy. J. Aircraft, vol. 8, no. 4, Apr. 1971, pp. 193-199.

5. Lamar, John E.: Extension of Leading-Edge-Suction Analogy to Wings With Separated Flow Around the Side Edges at Subsonic Speeds. NASA TR R-428, 1974.

6. Margason, Richard J; and Lamar, John E.: Vortex-Lattice FORTRAN Program for Estimating Subsonic Aerodynamic Characteristics of Complex Planforms. NASA TN D-6142, 1971.

7. Lamar, John E.; and Gloss, Blair B.: Subsonic Aerodynamic Characteristics on Interacting Lifting Surfaces With Separated Flow Around Sharp Edges Predicted by a Vortex-Lattice Method. NASA TN D-7921, 1975.

8. Lamar, John E.: Some Recent Applications of the Suction Analogy to Vortex-Lift Estimates. Aerodynamic Analyses Requiring Advanced Computers, Part II, NASA SP-347, 1975, pp. 985-1011.

9. Gersten, K.: Calculation of Non-Linear Aerodynamic Stability Derivatives of Aeroplanes. AGARD Rep. 342, Apr. 1961.

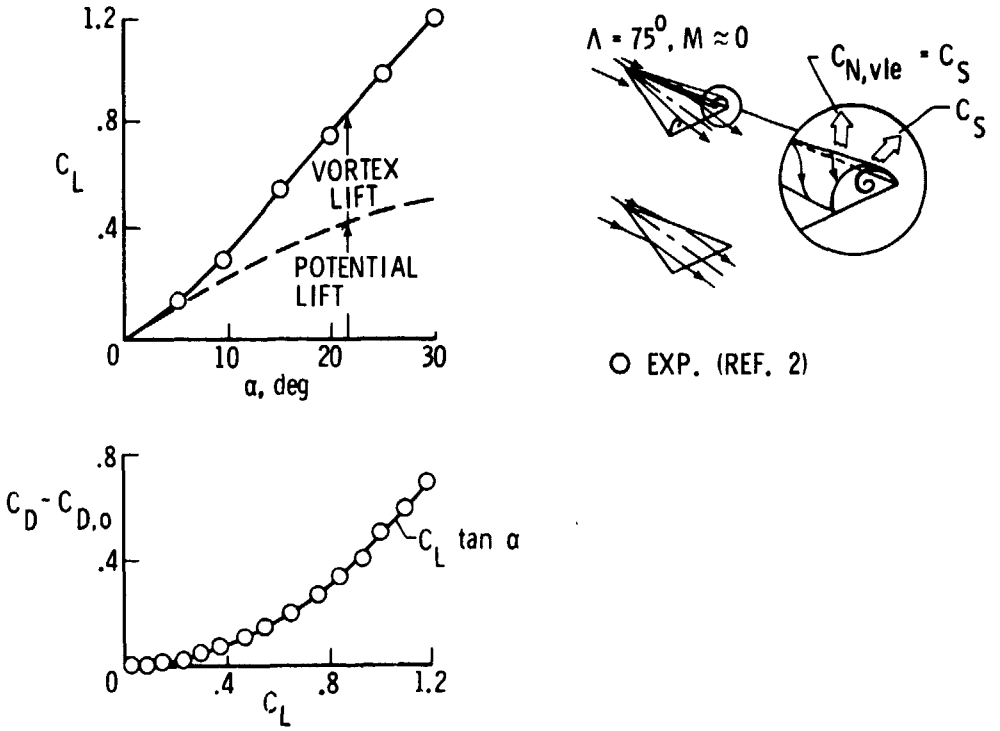

Figure 1.- Original application of leading-edge suction analogy.

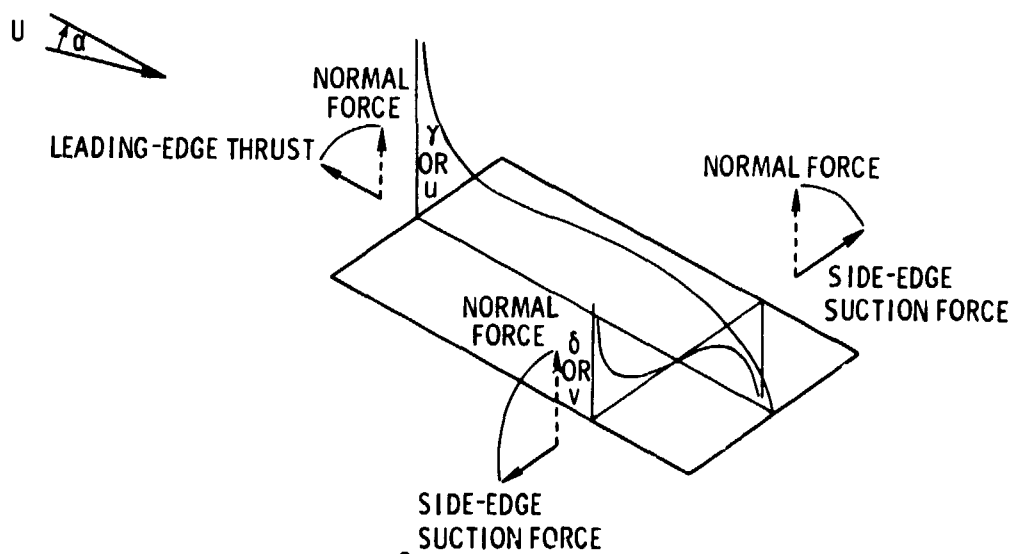

$$C_L = K_p \sin\alpha \cos^2\alpha + (K_{v,le} + K_{v,se}) |\sin\alpha| \sin\alpha \cos\alpha$$

Figure 2.- Vortex-lift concept: suction analogy application to leading edge and side edge.

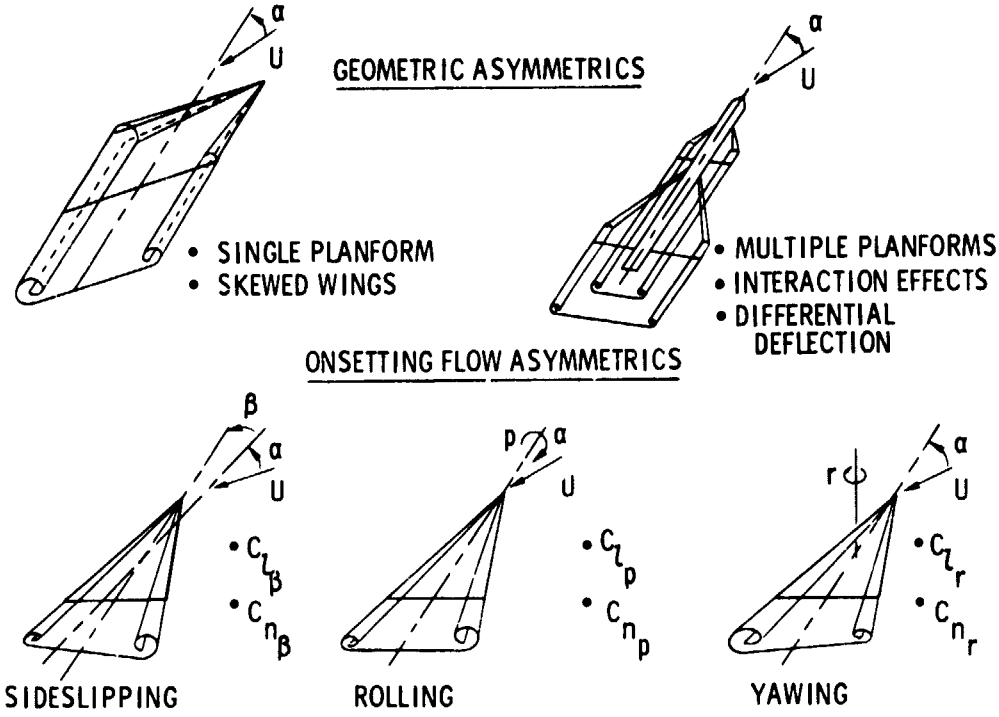

Figure 3.- Some recent applications of suction analogy to asymmetric vortex flow situations.

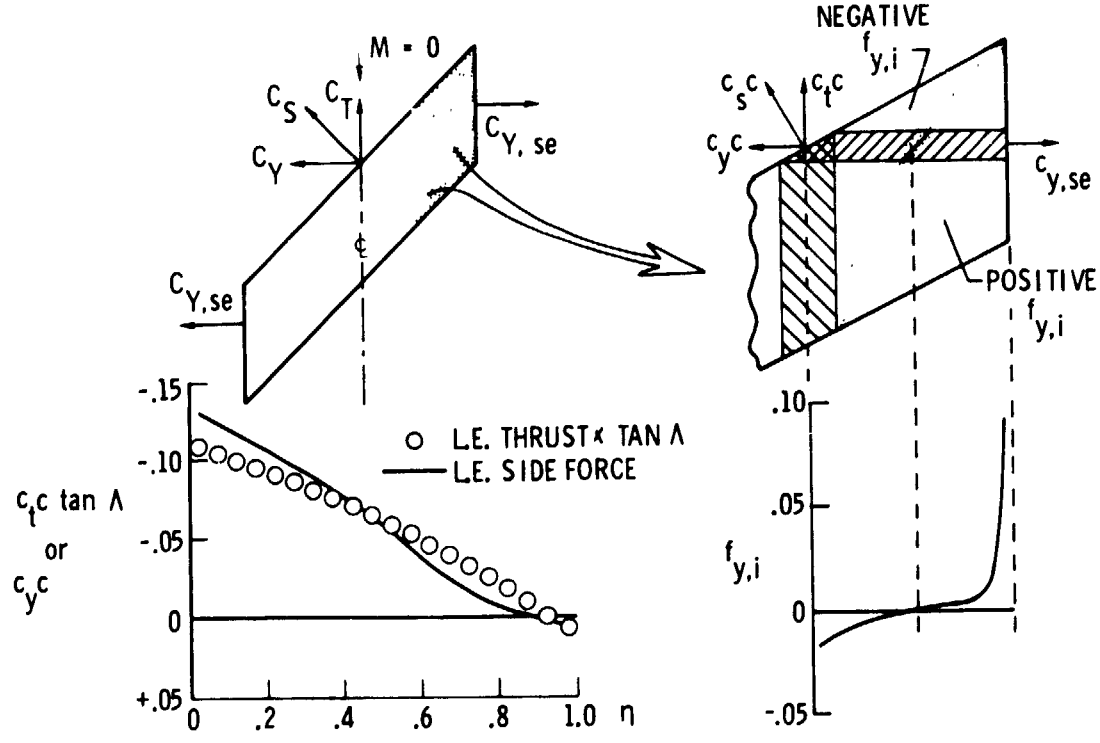

Figure 4.- Forward sweep effects on side-edge suction.

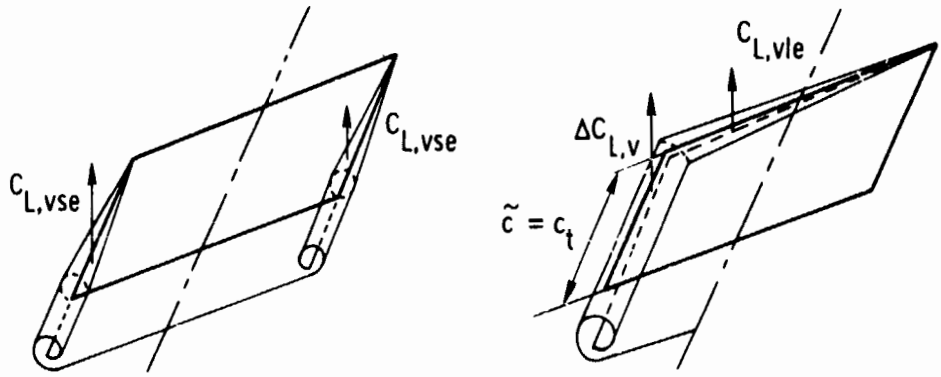

$$\bar{K}_{v,se} = \left(\frac{K_{v,le}}{b \sec \Lambda}\right)\tilde{c}$$

$$C_L = K_p \cos^2 \alpha \sin \alpha + (K_{v,le} + K_{v,se} + \bar{K}_{v,se}) |\sin \alpha| \sin \alpha \cos \alpha$$

Figure 5.- Concept of augmented vortex lift applied to a skewed wing.

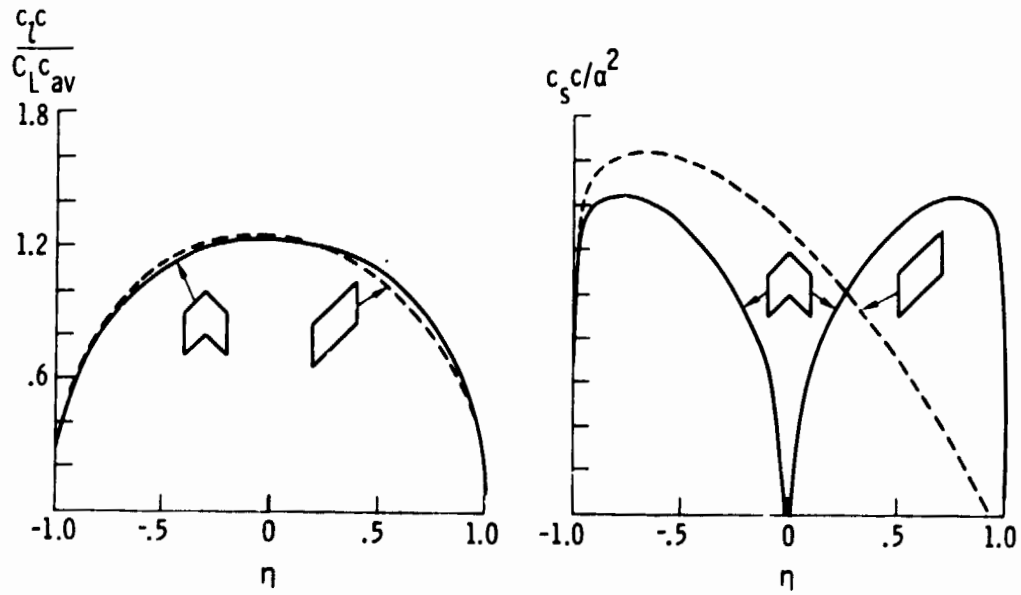

Figure 6.- Span load and section suction distributions on a swept and skewed wing. $\Lambda = 45^o$; $A = 1$; $M = 0$.

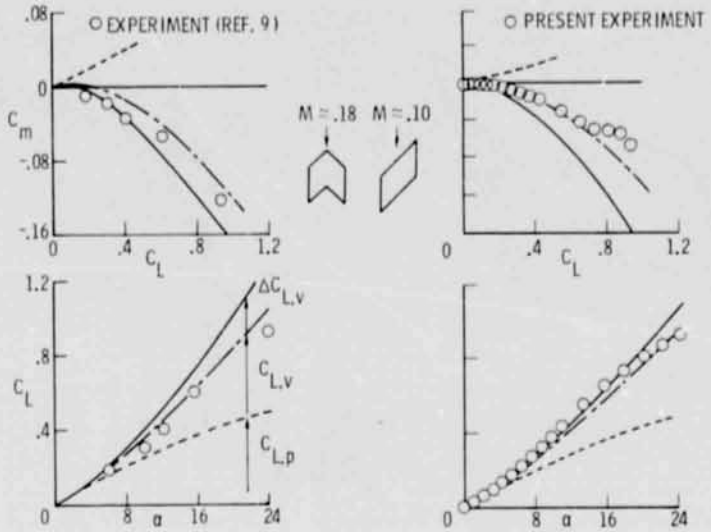

Figure 7.- Longitudinal characteristics of a swept and a skewed wing. $\Lambda = 45$; $A = 1$.

(a) $\Lambda = 45^{\circ}$; $A = 1$; $\alpha = 5^{\circ}$.

Figure 8.- Vortex flow on a skewed wing.

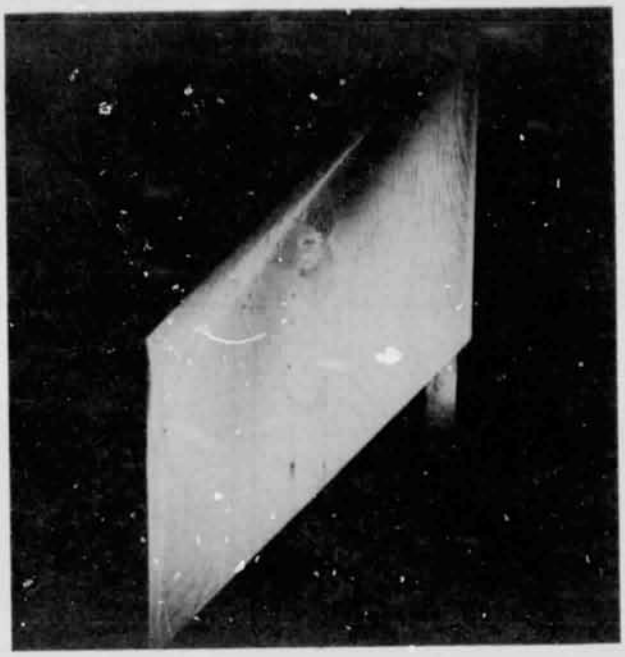

(b) $\Lambda = 45^{o}$; $A = 1$; $\alpha = 10^{o}$.

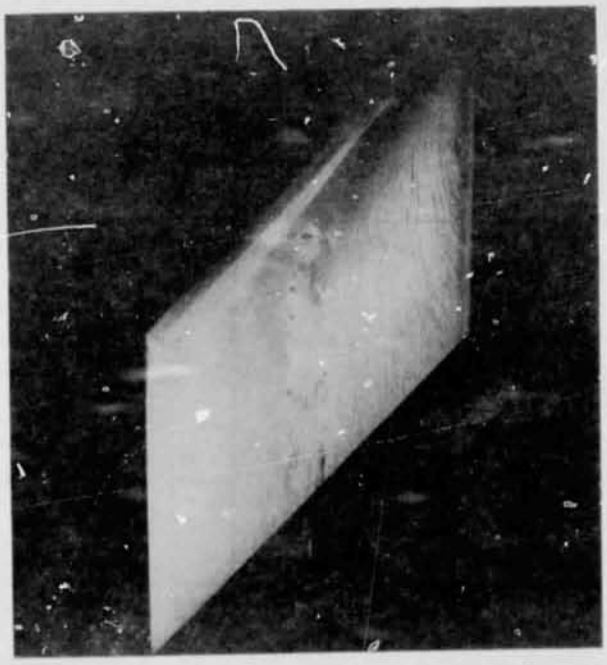

(c) $\Lambda = 45^{o}$; $A = 1$; $\alpha = 15^{o}$.

Figure 8.- Concluded.

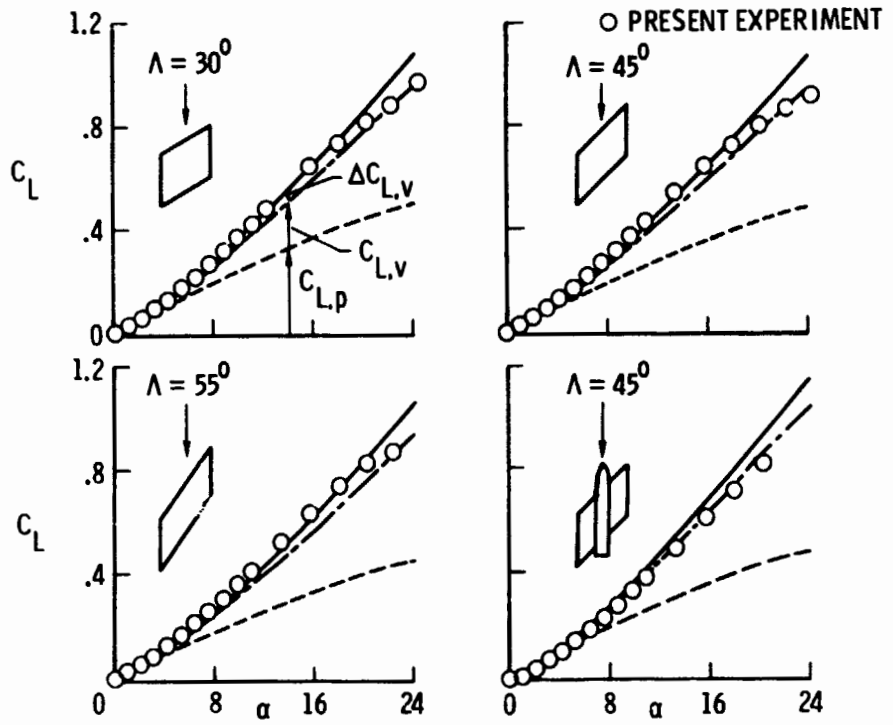

Figure 9.- Effect of leading-edge sweep on lift characteristics of several skewed wings. A = 1; M ≈ 0.10.

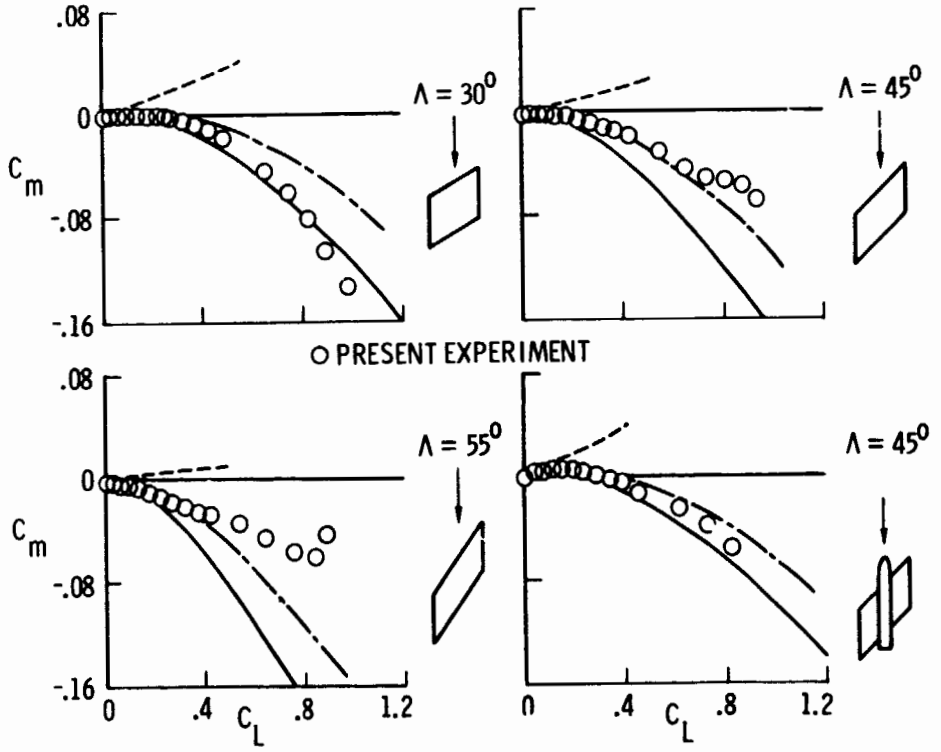

Figure 10.- Effect of leading-edge sweep on pitch characteristics of several skewed wings. A = 1; M ≈ 0.10.

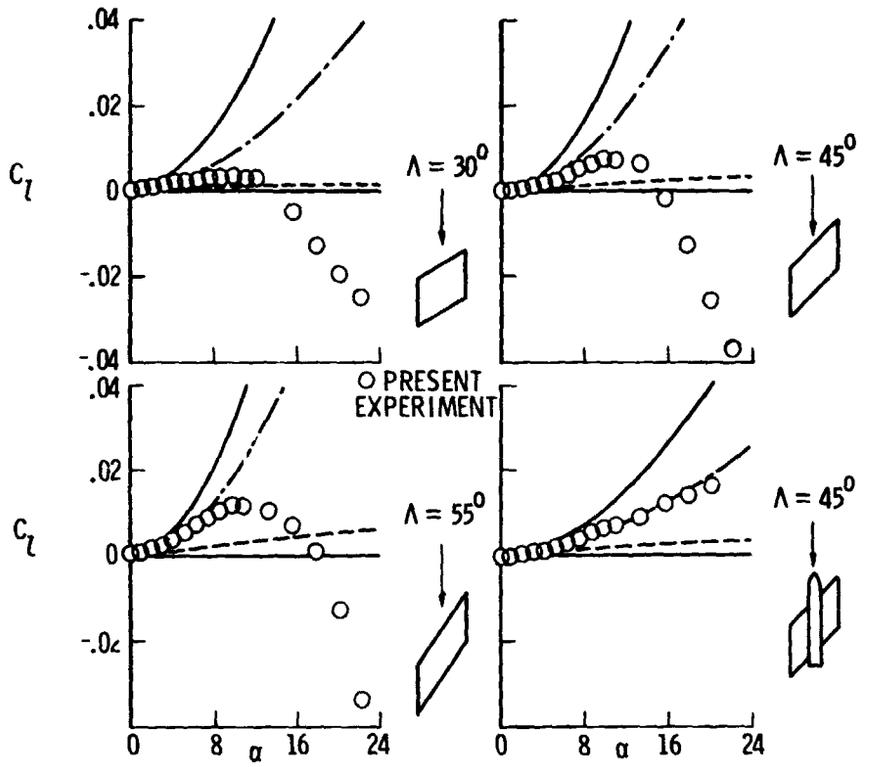

Figure 11.- Effect of leading-edge sweep on roll characteristics of several skewed wings. A = 1; M ≈ 0.10.

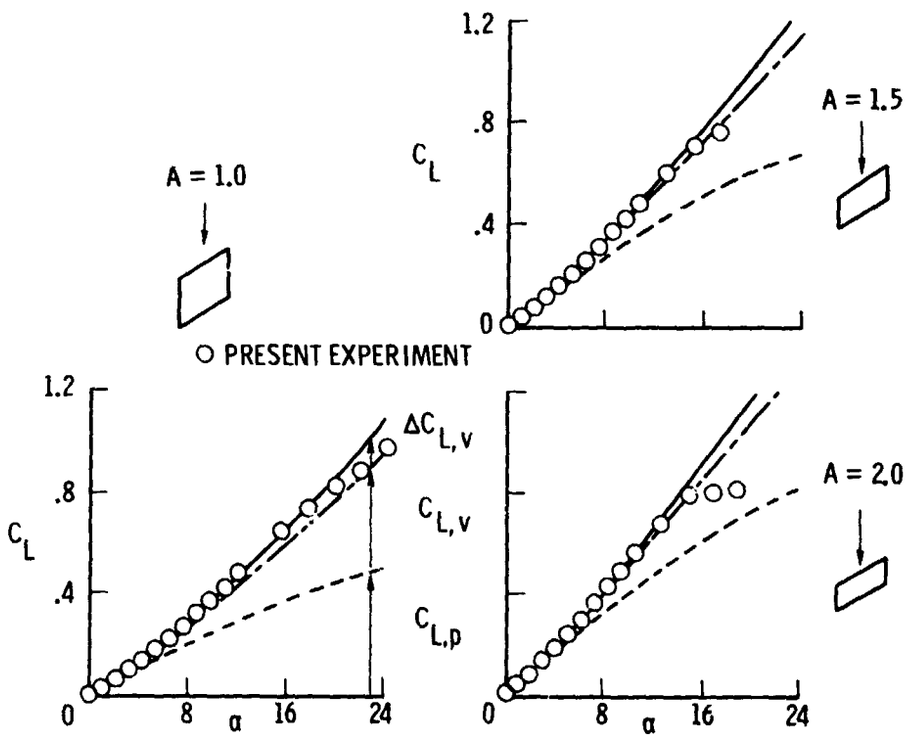

Figure 12.- Effect of aspect ratio on lift characteristics of several skewed wings. Λ = 30°; M ≈ 0.10.

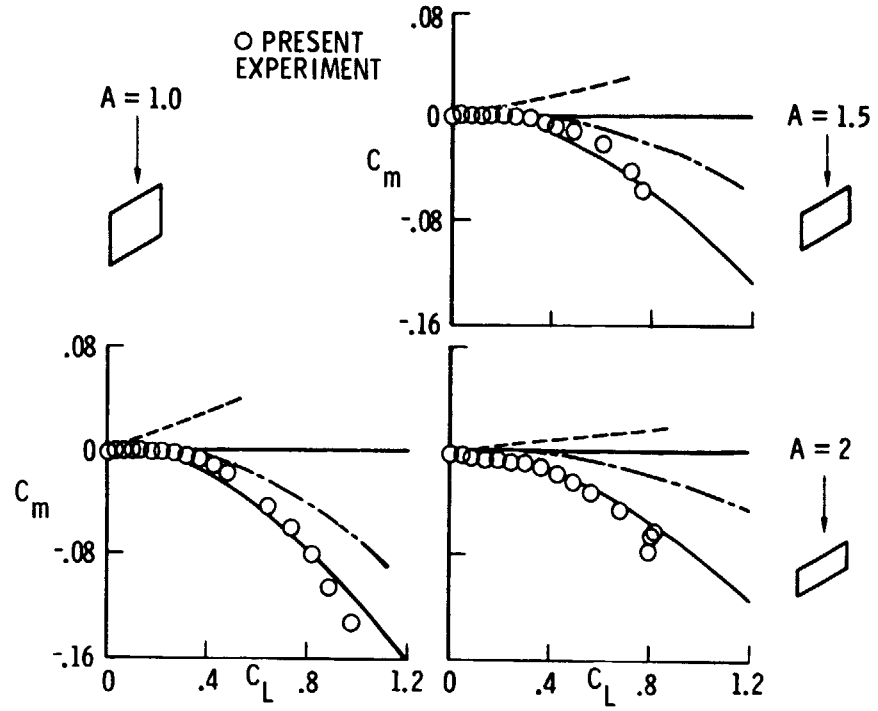

Figure 13.- Effect of aspect ratio on pitch characteristics of several skewed wings. $\Lambda = 30^{\circ}$; $M \approx 0.10$.

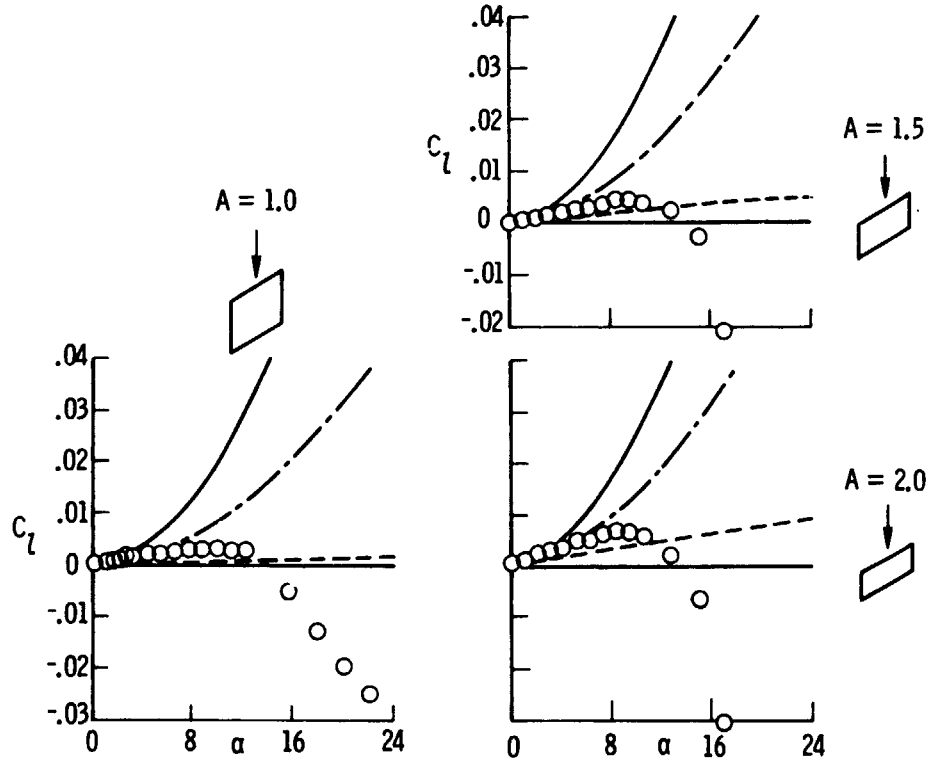

Figure 14.- Effect of aspect ratio on roll characteristics of several skewed wings. $\Lambda = 30^{\circ}$; $M \approx 0.10$.